Journal of Fluids and Structures (2002) **16**(2), 263–269
doi:10.1006/jfls.2001.0419, available online at http://www.idealibrary.com on IDEAL®

Special Communication
NEAR-WAKE FLOW STRUCTURE OF A CYLINDER WITH A HELICAL SURFACE PERTURBATION

C.-K. Chyu and D. Rockwell

Department of Mechanical Engineering and Mechanics, 354 Packard Laboratory 19 Memorial Drive West Lehigh University, Bethlehem, PA 18015, U.S.A.

(Received 7 May 2000, and in final form 22 August 2001)

The near-wake of a circular cylinder having a helical wire pattern about its surface is characterized using a technique of high-image-density velocimetry. Patterns of vorticity in three orthogonal planes show substantial influence of a wire having a diameter an order of magnitude smaller than the cylinder diameter. The distinctive patterns of vorticity in these three planes are associated with lack of formation of large-scale Kármán-like clusters of vorticity (ω_z) in the near-wake region of the cylinder. The instantaneous structure of the separating spanwise vorticity (ω_z) layers on either side of the cylinder involve small-scale concentrations of vorticity analogous to the well-known Kelvin–Helmholtz vortices from a smooth cylinder. Moreover, a dual vorticity layer, i.e., two adjacent layers of like vorticity (ω_z), can form from one side of the cylinder. Along the span of the cylinder, distributions of instantaneous velocity and transverse vorticity (ω_y) show a spatially periodic sequence of wake-like patterns, each of which has features in common with the very near-wake of a two-dimensional bluff body, including a large velocity defect bounded by vorticity layers with embedded small-scale vorticity concentrations. In the cross-flow plane of the wake, patterns of streamwise vorticity (ω_x) show small-scale, counter-rotating pairs of vorticity concentrations (ω_x) emanating from the inclined helical perturbation, rather than isolated concentrations of vorticity of like sign, which would indicate single streamwise vortices. All of the aforementioned patterns of small-scale vorticity concentrations are scaled according to the local wake width/local pitch of the helical wire pattern in the respective plane of observation.

1. INTRODUCTION

The use of surface modifications to alter the loading and vibration of a circular cylinder has been pursued in a wide range of investigations, as summarized by Zdravkovich (1981) and Naudascher & Rockwell (1994). These modifications take the form of, for example, straight and helical wires, staggered separation wires, and collars and rings. In addition, patterns of wires mounted away from the surface, as well as various configurations of perforated and axial-slat shrouds have received attention. Moreover, closely related to the present investigation are the works of Fage & Warsap (1929), Weaver (1961) and James & Truong (1972), who investigated the consequence of straight and helical surface perturbations. Nebres & Batill (1993) address the case of a circular cylinder with a single surface perturbation. The perturbation took the form of a small wire attached to the surface of the cylinder. The axis of the wire was parallel to the axis of the cylinder and, during the course of the experiments, the angular position of the wire was varied. The Strouhal number of vortex shedding and the time-averaged surface pressure distributions around the cylinder were determined as a function of angular position of the perturbation.

0889–9746/02/020263 + 07 $35.00/0

Stranded cables, which are woven from a number of wires, have an inherent pattern of surface nonuniformity, which takes a helical form. Such cables are employed in a range of practical scenarios. Underwater towing cables, mooring lines of ocean structures, overhead transmission lines, and cables on suspension bridges are subjected to steady and unsteady loading and vibration. Such loading, no doubt, is influenced by the type of surface nonuniformity of the cable. Nebres *et al.* (1993) considered the surface pressure profiles and the steady lift and normal drag for generic types of cables. Smoke visualization was employed to demonstrate that the separation process from the cable involved a cellular type of flow pattern. The smoke patterns suggested that streamwise vortical structures originated from the valleys of the helical strands of the cable. In an earlier investigation, Votaw & Griffin (1971) characterized the Strouhal numbers for unyawed vibrating cables. Other related investigations are summarized by Nebres *et al.* (1993).

All of the foregoing cases have involved geometrical modifications of the surface. A fluid analogy to a helical wire pattern about the surface of the cylinder was addressed by Lin *et al.* (1995). They employed a helical pattern of small holes about the surface of the cylinder and induced steady and unsteady injection of fluid through the surface. This approach led to substantial alterations of the patterns of near-wake vortex formation, which was characterized by high-image-density particle velocimetry. Even for relatively low values of fluid injection ratio, significant modifications of the near-wake were attainable, thereby suggesting that small geometrical surface perturbations are likely to be effective.

Despite the practical importance of geometrical surface perturbations on circular cylinders, the physics of the near-wake has received very little attention. The primary aim of the present investigation is to provide the first quantitative images of patterns of vorticity in orthogonal planes of the near-wake for the case of a helical surface perturbation. This type of approach can provide a basis for determining how surface perturbations alter the steady and unsteady loading and vibration.

2. EXPERIMENTAL SYSTEM AND TECHNIQUES

The experimental arrangement and methods are the same as those described by Chyu & Rockwell (1996); the present investigation was conducted in parallel with that effort. The reader is referred to this citation for details. Selected features are described herein.

A cylinder of diameter $D = 51{\cdot}1$ mm was fitted with a three-start helical perturbation, as illustrated in Figure 1; note that its diameter is not to scale, i.e., it has been enlarged relative to the scale of the cylinder. The perturbation was a flexible wire of diameter $0{\cdot}1D$, in which D is the diameter of the cylinder. It was glued to the surface of the cylinder. The local pitch P^* between successive crests of the helical winding was $P^* = P/3 = 1{\cdot}5$. This wire arrangement is shown in the right schematic of Figure 1. The length of the cylinder was 525 mm, and it was fitted with end plates at either end, as described by Chyu & Rockwell (1996). The cylinder was mounted horizontally at mid-depth in a large-scale free-surface water channel having a test-section 4880 mm long, 914 mm wide and 597 mm deep. The water level was maintained at 540 mm. The freestream velocity was 182 mm/s, yielding a value of Reynolds number $\mathrm{Re} = 10\,000$.

A technique of high-image-density particle image velocimetry (PIV) was employed; it is described in detail by Rockwell *et al.* (1993). A laser sheet was generated by rapidly scanning the beam from an argon-ion laser (4 W) to a rotating polygonal (72 facet) mirror. The scanning frequency was 626 cycles/s. An image-shifting mirror was located directly ahead of the camera lens system. The lens had a magnification factor $M = 1{:}2{\cdot}9$. The flow was seeded with 12 μm, metallic-coated hollow spheres. Multiply exposed images of the particles were recorded on high-resolution (35 mm) film, which was subsequently digitized at a resolution

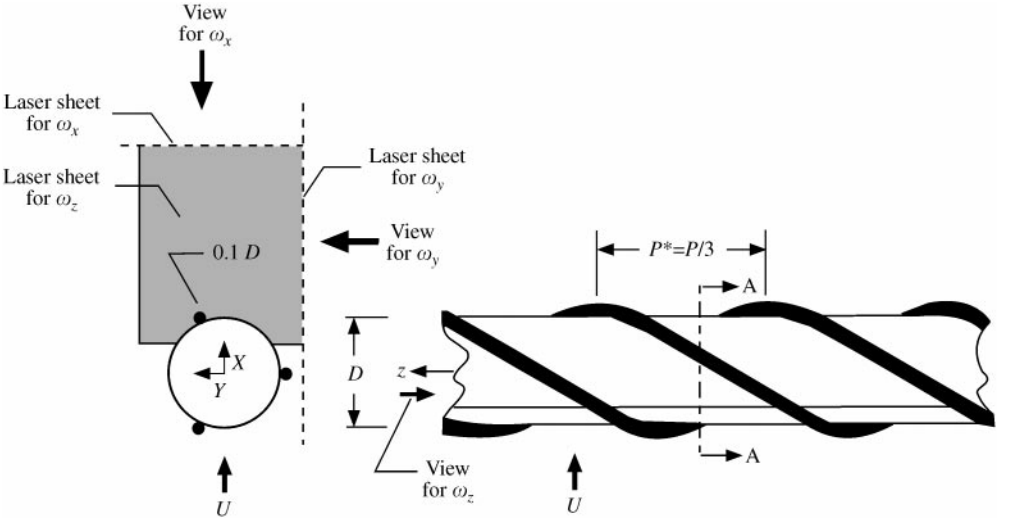

Figure 1. Schematic of the cylinder with a three-start helix about its surface; the diameter of the helical wire is drawn enlarged relative to the cylinder diameter. Also shown are orientations of the laser sheets for characterizing patterns of spanwise (ω_z), transverse (ω_y), and streamwise (ω_x) vorticity.

of 125 pixels/mm. The interrogation window was 100 pixels $\times$ 100 pixels. A single-frame cross-correlation approach was employed to evaluate the velocity field. The effective grid of the velocity vectors in the plane of the laser sheet was 1·25 mm.

The planes employed for imaging are designated in the left schematic of Figure 1. Laser sheet ω_z is orthogonal to the axis of the cylinder and thereby provides a quasi-two-dimensional representation of the vortex formation. Laser sheet ω_y is parallel to the axis of the cylinder and is positioned such that its edge just touches the surface of the helical wire; it yields images of the spanwise structure of the vortex formation, represented by transverse projections ω_y of the vorticity concentrations. A third orientation of the laser sheet is shown in Figure 1. It was parallel to the axis of the cylinder and oriented such that it was coincident with the cross-flow plane of the near-wake, thereby providing instantaneous streamwise projections ω_z of the vorticity concentrations.

In each of the images presented herein, the minimum and incremental values of positive and negative vorticity are the same, but their numerical values are not specified. For example, in each image representing patterns of positive and negative spanwise vorticity ω_z, vorticity levels can be cross-compared. Moreover, vorticity levels can be cross-compared between various images of ω_z in a given layout of images.

3. EXPERIMENTAL RESULTS

3.1. Patterns of Spanwise Vorticity (ω_z)

Figure 2(a) shows a representative pattern of instantaneous spanwise vorticity from the smooth cylinder for the field of view defined in the left schematic of Figure 1. It is evident that large-scale Kármán vortices are formed in the near-wake region due to the abrupt coalescence of small-scale shear-layer vortices that develop in the separating shear layers (Chyu & Rockwell 1996).

The images of Figure 2(b) show that, in the presence of the helical perturbation, this large-scale vortex formation is completely inhibited in the near-wake region. Furthermore,

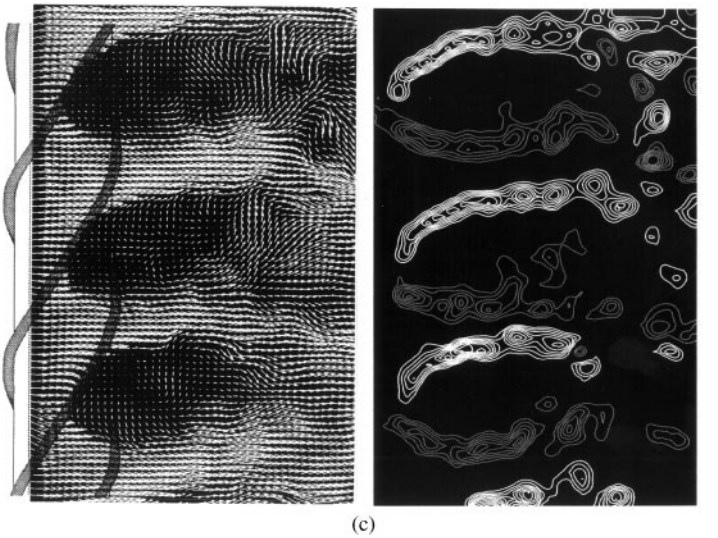

(c)

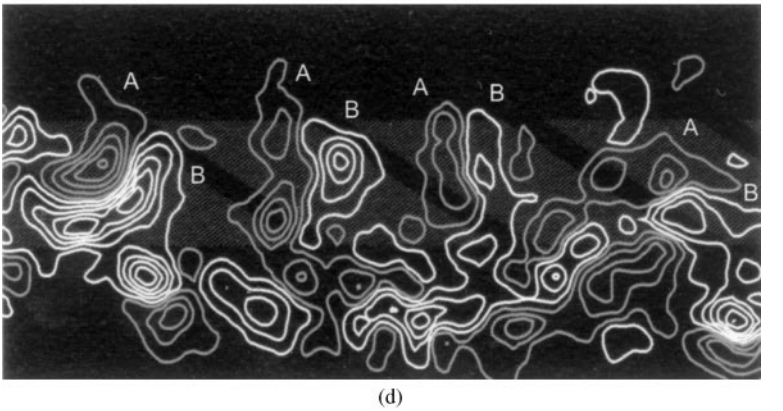

(d)

Figure 2(c). Patterns of instantaneous velocity and vorticity ω_y, which correspond to the laser sheet orientation designated as ω_y in Figure 1. Height of each image is 5·4D. Re = 10 000. (d) Patterns of instantaneous streamwise vorticity ω_x obtained by orienting the laser sheet in the cross-flow plane of the near-wake of the cylinder, as indicated in Figure 1. The laser sheet is located at $x/D = 2$. The centerline of the cylinder is coincident with the center of the image, and the height of the image corresponds to 3D. Re = 10 000.

all images indicate that the vorticity layers tend to merge together over the streamwise extent of the image, and the central portion of the wake region tends to be vorticity-free, relative to the vorticity levels in the separating shear layer, indicating that no intermittent large-scale vortex formation occurs near the base of the cylinder during times earlier than those at which the images were acquired. By rotating the entire cylinder to different angular positions, it was possible to determine the localized structure of the shear layers separating from the cylinder, as indicated in Figure 2(b). This structure is, of course, dependent upon the angular location of the helical perturbations at the cross-section of interest. In each image, the sectional cut of the helical perturbation is designated by the small circular symbol immediately adjacent to the large cylinder. Three such circular symbols are symmetrically located about the circumference of the cylinder; only the symbol closest to the base of the cylinder is shown in each image.

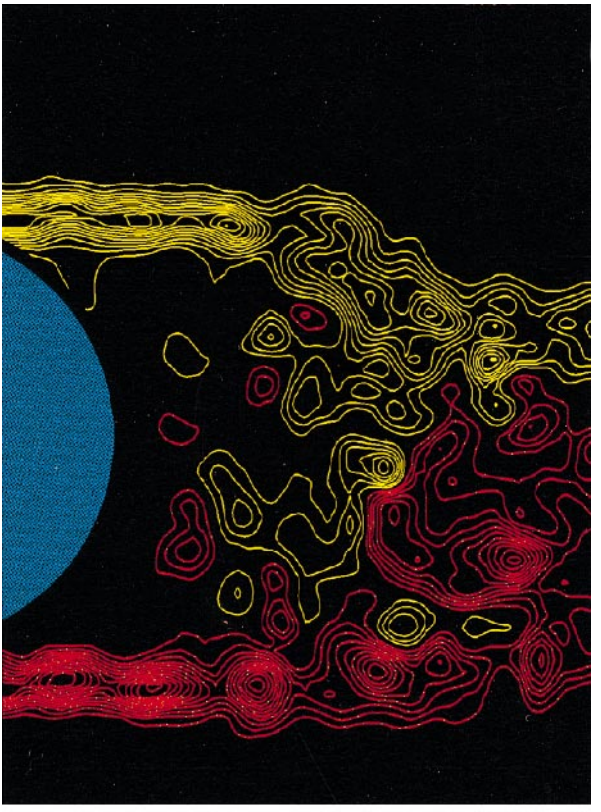

(a)

Figure 2(a). Patterns of instantaneous concentrations of spanwise vorticity ω_z for the case of a smooth cylinder. Re = 10 000.

doi:10.1006/20010419

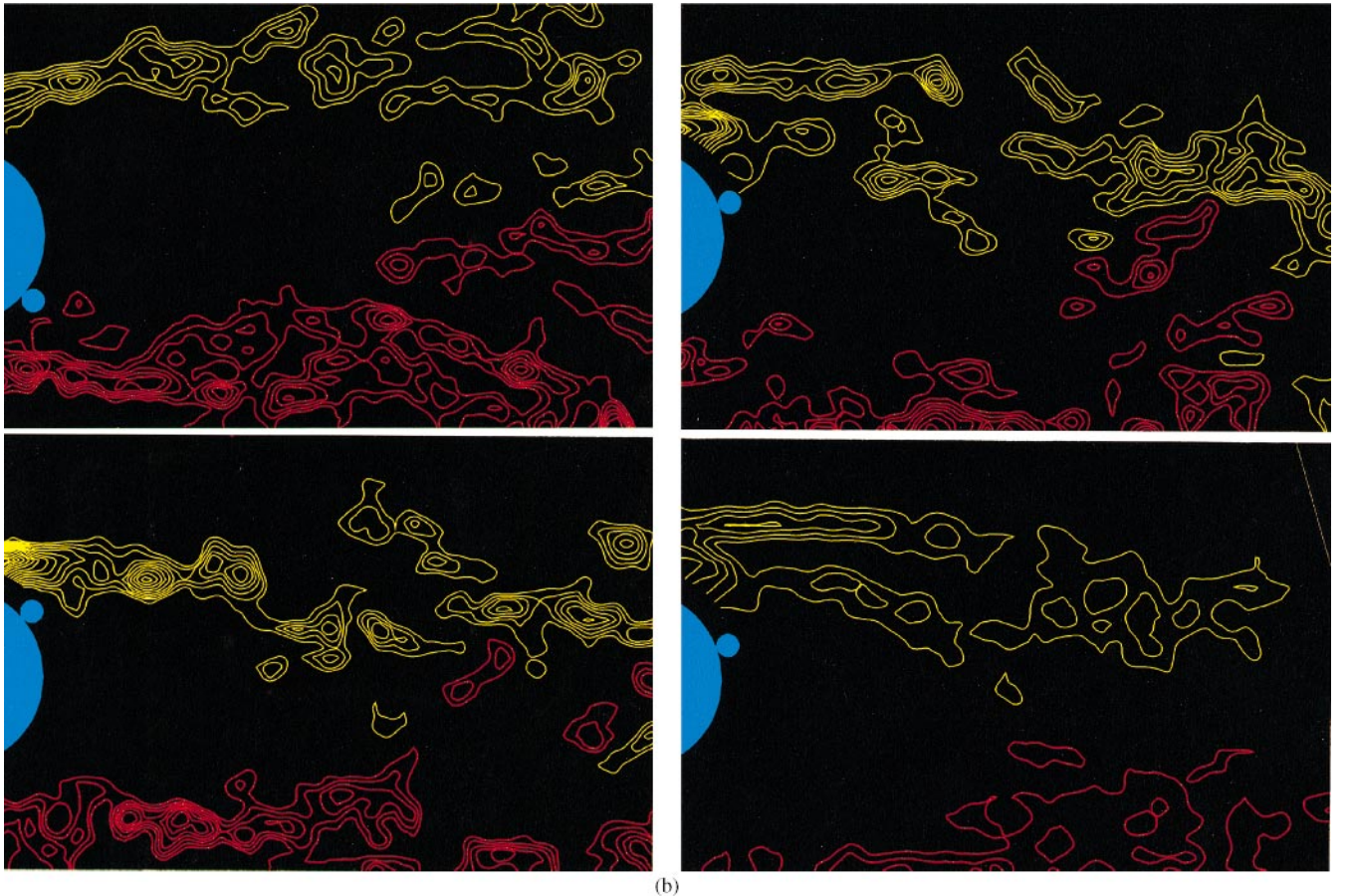

(b)

Figure 2(b). Patterns of spanwise ω_z vorticity with the three-start helix on the surface of the cylinder. Images show the locations of cross-sections of the helical wires at different angular positions, which were obtained by rotation of the cylinder. Images at the upper and lower left, and at the upper right, show instantaneous patterns. The bottom right image is an average of instantaneous images corresponding to the sectional cut of the upper right image. Re = 10 000.

doi:10.1006/20010419

The image at the upper left of Figure 2(b) corresponds to the case where the sectional cut of the helical wire, i.e., the small circular symbol, is on the lower right of the base region of the cylinder. In this case, the separating vorticity layers are nearly symmetrical with respect to the plane of symmetry of the wake of the cylinder; moreover, they tend to diverge in the near-wake region. This effect is apparently due to nearly symmetrical separation induced at the two sectional cuts of the helical pattern, which are not visible in the image layout.

On the other hand, when the cylinder is rotated to the orientation shown in the image at the bottom left of Figure 2(b), the pattern of vorticity layers becomes markedly asymmetrical. In concept, a similar type of asymmetrical separation, based on qualitative smoke visualization, is evident in the schematic of Nebres *et al.* (1993) for the case of a stranded cable. The degree of asymmetry was strongly dependent upon the angular locations of the sectional cuts of the cable winding.

A remarkable form of the vorticity pattern is generated when the cylinder is rotated to the position corresponding to the upper right image of Figure 2(b). In this case, there are two distinct layers of instantaneous negative vorticity from the upper surface of the cylinder. This dual layer structure is apparently associated with: (i) separation from a section of the helical perturbation on the fore surface of the cylinder (not visible in the image); and (ii) separation from the section of the perturbation shown in the image. The corresponding averaged image, obtained from the three instantaneous images, is shown at the lower right. The general form of the dual-layer structure is remarkably similar in the instantaneous and averaged images.

The effective width of the near-wake is defined as the transverse distance between separated vorticity layers, at a location of one-half wake width downstream of the base of the cylinder. This width varies substantially between each of the instantaneous images of Figure 2(b). The narrowest wake is at the sectional cut represented by the image at the bottom left. The wake width of the top left image is larger by 20% and the width of the top right image is larger by 37%. The substantial differences of the effective width of the wake suggest large spanwise variations in the instantaneous flow pattern along the span. As will be discussed in Section 3.2, this is indeed the case.

A common feature of all of the separated layers exhibited in the instantaneous images of Figure 2(b) is the occurrence of small-scale vortical structures. For the corresponding case of shear layer formation from the smooth cylinder, shown in Figure 2(a), these small-scale structures arise from a Kelvin–Helmholtz instability of the separating shear layer, as addressed in detail by Chyu & Rockwell (1996) and references discussed therein. In the image of Figure 2(a), the streamwise wavelength λ of these small-scale concentrations of vorticity, relative to the width D_w of the very near wake, is $\lambda/D_w \cong 0{\cdot}20$. For the patterns of Figure 2(b), localized flow separation induced by the inclined surface perturbation yields well-defined small-scale concentrations of vorticity. They are, however, not in the form of an orderly train of vortices as for the case of the smooth cylinder Figure 2(a). Nevertheless, it is possible to define a streamwise wavelength between vorticity concentrations normalized with respect to the local wake width D_w. These values are in the range of $0{\cdot}17 < \lambda/D_w \leq 0{\cdot}39$.

3.2. Patterns of Transverse Vorticity (ω_y)

Further insight into the effect of the helical perturbation is obtained by the acquisition of instantaneous patterns of velocity and vorticity using the laser sheet orientation designated as ω_y in the schematic of Figure 1. For the images shown in Figure 2(c), the edge of the laser sheet just touches the surface of the helical wire. The left image shows a pattern of instantaneous velocity and the right image provides the corresponding instantaneous

vorticity ω_y. The instantaneous velocity vectors show that the helical perturbation produces a spatially periodic pattern of wake-like flows along the span of the cylinder. In each wake-like region, patterns of nearly zero, or even negative flow, are generated. The center of each wake-like region is approximately coincident with the crest of each helical perturbation, and the width of each region grows very rapidly from its inception at the crest of helical perturbation. The effective width D_w of each of these wake-like regions is approximately equal to the cylinder diameter, i.e., $D_w \simeq D$.

The corresponding pattern of instantaneous vorticity shows concentrated layers along the edges of each wake-like region. The vorticity level of the positive (white) layer is slightly higher than its corresponding negative (gray) layer, i.e., the peak values in the white layer exceed those in the gray layer by a factor of approximately 1·4, no doubt due to the inclination of the helical winding shown in the schematic of the corresponding image. The patterns of velocity and vorticity of a typical wake-like region show widely separated layers of opposite sense, which bound a low velocity region and contain small-scale concentrations of vorticity. In these respects, a given wake-like region resembles the very near-wake from a two-dimensional bluff body. The ordered sequences of small-scale vorticity concentrations in the layers along the edges of the wake-like regions, shown in Figure 2(c), have a well-defined streamwise wavelength λ, which can be normalized with respect to the local wake width D_w in this view. It has values in the range $0{\cdot}45 \leq \lambda/D_w \leq 0{\cdot}55$.

3.3. Patterns of Streamwise Vorticity (ω_x)

Images acquired in a plane parallel to the axis of the cylinder and orthogonal to the free-stream allow visualization of patterns of streamwise vorticity ω_x. In other words, the laser sheet was oriented such that it visualized the cross-flow plane in the near-wake region. A pattern of instantaneous streamwise vorticity ω_x is shown in Figure 2(d). It is evident that identifiable concentrations of ω_x exist along the upper region of the image. These vorticity concentrations take the form of counter-rotating vortex pairs, that is, vorticity concentrations A and B immediately adjacent to each other. The spanwise wavelength between these counter-rotating vorticity concentrations is approximately equal to the wavelength of the helical perturbation.

4. CONCLUDING REMARKS

The present investigation shows that a three-start helical wire, which has a diameter one order of magnitude smaller than the diameter of the cylinder on which it is mounted, can preclude the rollup of spanwise vorticity into large-scale clusters, i.e., the formation of Kármán vortices, in the near-wake region. This overall modification of the near-wake is associated with distinctive patterns of vorticity in all three orthogonal planes in the near-wake.

Sectional cuts of the quasi-two-dimensional (spanwise) vorticity layers ω_z taken at different spanwise locations of the helical perturbation show: substantial variation of the effective wake width; existence of a dual (two) vorticity layer; and small-scale concentrations of vorticity, which resemble the well-known Kelvin–Helmholtz vortices from a smooth cylinder. The streamwise wavelength between these small-scale concentrations, normalized by the effective wake width, is generally larger than the corresponding dimensionless wavelength in the separated shear layers from a smooth cylinder. For the latter case, it is known that the existence of small-scale concentrations can markedly alter the Reynolds stresses and entrainment demands of the shear layers. A productive extension of the present study would address the relation between the time-averaged structure of the near-wake,

including the spacing of the separated layers, in relation to the generation and interaction of small-scale concentrations of vorticity.

The spanwise structure of the near wake, represented by patterns of velocity and transverse vorticity ω_y, shows spatially periodic, wake-like regions. They are formed at the crest of the helical perturbation, and rapidly increase in width. The principal features of a given wake-like region are: widely spaced vorticity layers of opposite sense, which contain small-scale concentrations of vorticity having a well-defined wavelength; and a large velocity defect between the layers. In these respects, each wake-like region mimics the wake from a two-dimensional bluff body at sufficiently high Reynolds number. These observations suggest that the attenuation of large-scale quasi-two-dimensional Kármán vortices in the near-wake of the cylinder may be significantly influenced by the existence of these wake-like regions along the span, and are not simply due to the generation of streamwise vorticity from each crest of the helical perturbation.

A further representation of the spanwise structure involves concentrations of streamwise ω_x vorticity in the near-wake region. They suggest the existence of streamwise vortices, which are generated from the inclined segment of the helical perturbation at the shoulder of the cylinder. Counter-rotating vortex pairs, rather than single streamwise vortices, appear to be generated in the near-wake. The wavelength between these pairs is approximately equal to the spanwise distance between successive crests of the helical perturbation on the cylinder. The strength of these streamwise concentrations, relative to the scale and angle of inclination of the helical perturbation, is currently under investigation.

ACKNOWLEDGEMENTS

The authors gratefully acknowledge financial support of the Office of Naval Research through Grant N00014-94-1-0185, monitored by Dr Thomas Swean. Supplemental support was provided by the National Science Foundation under Grant CTS-9803734, monitored by Dr John Foss.

REFERENCES

CHYU, C.-K. & ROCKWELL, D. 1996 Near-wake structure of an oscillating cylinder: effect of controlled shear-layer vortices. *Journal of Fluid Mechanics* **332,** 21–49.

FAGE, A. & WARSAP, J. 1929 The effects of turbulence and surface roughness on the drag of a circular cylinder. British ARC R&M 1283.

JAMES, D. & TRUONG, Q. 1972 Wind load on cylinder with spanwise protrusion. *ASCE Journal of the Engineering Mechanics Division* **98,** 1573–1589.

LIN, J.-C., TOWFIGHI, J. & ROCKWELL, D. 1995 Instantaneous structure of near-wake of a circular cylinder: On the effect of Reynolds number. *Journal of Fluids and Structures* **9,** 409–418.

NAUDASCHER, E. & ROCKWELL, D. 1994 *Flow-Induced Vibrations*: *An Engineering Guide*. Rotterdam: A. A. Balkema Press.

NEBRES, J. & BATILL, S. 1993 Flow about a circular cylinder with a single large-scale surface perturbation. *Experiments in Fluids* **15,** 369–379.

NEBRES, J., BATILL, S. & NELSON, R. 1993 Flow about yawed, stranded cables. *Experiments in Fluids* **14,** 49–58.

ROCKWELL, D., MAGNESS, C., TOWFIGHI, J., AKIN, O. & CORCORAN, T. 1993 High image-density particle image velocimetry using laser scanning techniques. *Experiments in Fluids* **14,** 181–192.

VOTAW, C. W. & GRIFFIN, O. M. 1971 Vortex shedding from smooth cylinders and stranded cables. *Transactions of the ASME*, *Journal of Basic Engineering* **93,** 457–460.

WEAVER, W. 1961 Wind-induced vibrations in antenna members. *ASCE Journal of the Engineering Mechanics Division* **87,** 141–165.

ZDRAVKOVICH, M. 1981 Review and classification of various aerodynamic means for suppressing vortex shedding. *Wind Engineering and Industrial Aerodynamics* **7,** 145–189.